Knowledge-Based Systems 81 (2015) 117–130

Contents lists available at ScienceDirect

Knowledge-Based Systems

journal homepage: www.elsevier.com/locate/knosys

Multi-modal fusion of palm-dorsa vein pattern for accurate personal authentication

Puneet Gupta [a,*], Phalguni Gupta [b]

[a] Department of Computer Science and Engineering, Indian Institute of Technology Kanpur, Kanpur 208016, India
[b] National Institute of Technical Teachers' Training and Research, Kolkata, Kolkata 700106, India

ARTICLE INFO

Article history:
Received 6 October 2014
Received in revised form 31 January 2015
Accepted 5 March 2015
Available online 14 March 2015

Keywords:
Biometrics
Vein pattern
Authentication
Verification
Multi-modal fusion

ABSTRACT

This paper proposes an efficient multi-modal authentication system which makes use of palm-dorsa vein pattern. There are four levels of fusion in the system and they are multi-algorithm fusion, data fusion, feature fusion and score fusion. Multi-algorithm fusion is applied to extract genuine vein patterns from a vein image by using various vein extraction algorithms. All false vein patterns are eliminated from the extracted patterns through data fusion. Three types of features are obtained from each extracted vein pattern and they are shape features, minutiae and features obtained from hand boundary shape. Third level of fusion is at feature level to fuse minutiae and shape features. Finally, fused features and hand boundary shape features are matched to obtain matching scores which are fused at score level. The proposed system has been tested on the database acquired from 4120 images of 1030 subjects. It has achieved an accuracy of 100%. Experimental results reveal that it performs better than other existing systems.

1. Introduction

Data protection or security is a major concern in today's digital age because of the availability of large digital data and cheap hardware. Methods based on keys or passwords are not useful because these can be easily spoofed, lost, forgot or stolen. Thus, use of biometrics is proliferated which recognizes an individual based on his/her characteristics [1]. One such biometric trait is a vein pattern which is the formed by the subcutaneous blood vessels. Like any other biometric trait, it has all the properties required in a recognition system, viz., universality, uniqueness [2], permanence [3] and acceptability [4]. In addition, it has the following properties [5] which escalated its utilization in personal authentication: (i) it can be acquired in a contact-less manner; (ii) it assures liveness; (iii) it is hard to forge as it lies inside skin; (iv) it can be easily and instantaneously acquired by using cheap sensors; and (v) it is highly user friendly. Motivated by all these factors, a personal authentication system based on vein pattern is proposed in this paper.

A vein pattern image acquired from X-ray or ultrasonic scanners (in medical imaging) has high quality. But it is highly user inconvenient due to slow acquisition and thus, avoided for biometric purposes. It is observed that areas containing vein pattern have dark intensities as compared to its surrounding tissues when observed under infrared (IR) light because IR light is absorbed by the blood flowing in the veins [6]. Thus, IR imaging is used in the biometrics for contact-less and non-invasive acquisition of vein images. However, genuine veins can be missed or spurious veins can be generated due to the following reasons: (i) skin properties (like the thickness, texture and hairs) [7]; (ii) environmental conditions (like temperature); (iii) non-uniform illumination [8]; (iv) varying width veins; and (v) low local contrast.

This paper proposes an efficient vein pattern based personal authentication system. Its research contributions and underlying motivations are:

1. Vein enhancement is a challenging problem due to variable width veins, low local contrast, non-uniform illumination and skin properties (like hairs). Thus, a hair removal algorithm and multi-scale matched filtering are used for vein enhancement. Also, global thresholding is not useful for vein extraction because it can miss the genuine veins. In contrast, local thresholding can generate spurious veins. Therefore, multi-algorithm fusion of local and global thresholding is proposed in this paper for better vein extraction. In addition, multi-scale matched filtering is used to handle the effects of variable width veins, low local contrast and non-uniform illumination.

* Corresponding author.
E-mail addresses: puneet@cse.iitk.ac.in (P. Gupta), director@nitttrkol.ac.in (P. Gupta).

http://dx.doi.org/10.1016/j.knosys.2015.03.007
0950-7051/

2. This paper commences the use of data fusion for removing spurious vein pattern during enrollment. This helps to remove spuriously generated veins and cavities while retaining the true veins.
3. Local features or shape features can be used for vein matching but their performance is restricted. It is because local features like minutiae cannot be accurately extracted and localized in the vein pattern while shape matching fails when spurious veins are generated or genuine veins are missed. Thus, three different types of features, viz., vein shape, minutiae bifurcations and hand boundary are used in this paper to achieve better performance. Some part of palm-dorsa boundary is found to be stable because of the presence of bones. Use of boundary features is also initiated in this paper.
4. A hybrid fusion strategy is proposed in this paper to design an accurate vein pattern based authentication system. Minutiae and shape features are fused to obtain a feature fused image by using feature level fusion. Feature fused image and boundary features are eventually fused by using score level fusion.

The paper is organized as follows. Next section has discussed some of the well known vein pattern based recognition algorithms. An efficient vein pattern based authentication system has been proposed in Section 3. Its performance has been evaluated on IITK database of 4120 images acquired from 1030 subjects. Experimental results have been analyzed in Section 4. Conclusions are given in the last section.

2. Related work

A vein biometric based authentication system mainly consists of vein enhancement, vein extraction, feature extraction and feature matching.

2.1. Vein enhancement and extraction

Palm-dorsa image is enhanced before vein extraction to minimize the effects of low local contrast, non-uniform illumination and noise present in the acquired vein images. Filtering based on Steerable filter [9], Gabor filter [10], Curvelet filter [11] and Retinex [12] can be used for vein enhancement. These are based on the shape of local neighborhoods of vein pattern and hence perform poorly for variable width veins. Vein tracking relies on the principle that by using local minima, vein area can be tracked from a large number of locations as opposed to the background areas [13]. For better performance, maximum curvature information can be used along with vein tracking [14]. Since thin veins can be tracked from fewer locations, these may be missed. Further, spurious veins can be generated due to avoidance of local vein shape during vein tracking. Scattering effect in IR imaging can be reduced by using restoration algorithms [15,16]. Global [17] and local [18] thresholding are applied to the enhanced vein image to extract the vein pattern. Global thresholding perform poorly if significant overlap exists between the intensities of background and foreground pixels. In contrast, local adaptive thresholding performs poorly when local neighborhoods do not have significant variation. Various features are extracted from the vein pattern which are used for vein matching.

2.2. Feature extraction and matching

Local or global features are extracted from the vein pattern and used for matching. Local features refer to the geometrical transformation invariant points [19]. Vein endings and bifurcations are commonly used local features which can be extracted by applying crossing number technique [20] on vein pattern. Extracted minutiae can be represented as features by various ways, such as distances among minutiae pairs [21], minutiae triangulations [22] and orientation [23]. But such representations are error prone because minutiae cannot be accurately localized in vein pattern. Minutiae matching can be carried out by using point-to-point matching algorithms like line segment hausdorff distance (*LHD*) [6] and modified hausdorff distance (*MHD*) [24]. But such matching algorithms are highly sensitive to geometrical transformation. Thus, spectral minutiae representation [25,26] can be used which requires global matching. Usefulness of minutiae features for vein matching is restricted because (1) sometimes few genuine minutiae are available; (2) minutiae location cannot be accurately determined; and (3) sometimes spurious minutiae can be generated due to noise generated by hair and texture. Vein matching can also been done using its shape or global feature. Extracted vein patterns can be matched by using pixel-by-pixel matching [27]. Local binary patterns of extracted vein are matched by using chi-square statistic [28]. Likewise, dilated skeleton can be matched by using correlation [29]. *LHD* is also useful for matching the vein skeletons [30]. Global features in vein pattern can be given by phase information [31] and texture analysis [32]. Global matching can give wrong results due to following reasons: (i) sometime thin vein pattern can be missed out; (ii) some spurious veins can be generated due to hair, noise, texture and non-uniform illumination; (iii) there are errors in localization of extracted vein and skeleton.

3. Proposed system

In this section, a palm-dorsa vein pattern based authentication system is proposed. It consists of six major stages which are (i) vein extraction, (ii) data fusion, (iii) feature extraction, (iv) feature level fusion, (v) feature matching, and (vi) score level fusion. In the first stage, palm-dorsa image is acquired and vein pattern present in it is extracted. In case of enrollment, two palm-dorsa images are acquired and there vein patterns are extracted. These are fused in the data fusion stage to remove the spurious veins. In the next stage, minutiae and boundary features are extracted from the vein pattern. Feature level fusion is done to fuse shape of vein pattern and minutiae features in the subsequent stage. It is followed by the feature matching stage where matching scores for different features are obtained. Score level fusion is done to obtain the matching scores. Its flow-graph is given in Fig. 1.

3.1. Vein extraction

This section consists of three major stages: (i) image acquisition; (ii) region extraction and preprocessing; and (iii) multi-algorithm fusion for vein extraction. Palm-dorsa image is acquired by using the acquisition setup. Its palm-dorsa area referred as region of interest (ROI) is extracted and enhanced. Veins are extracted from the enhanced image by using a multi-algorithm fusion strategy.

3.1.1. Image acquisition

The acquisition setup is enclosed in a box to minimize environmental interference. Palm-dorsa part of the human hand is illuminated by two IR lamp of wavelength 850 nm. An SLR camera is used to acquire vein images which assures high resolution image. The box has

1. a hole on the top where SLR camera is placed,
2. a hole in a side wall from which a hand can slip in,

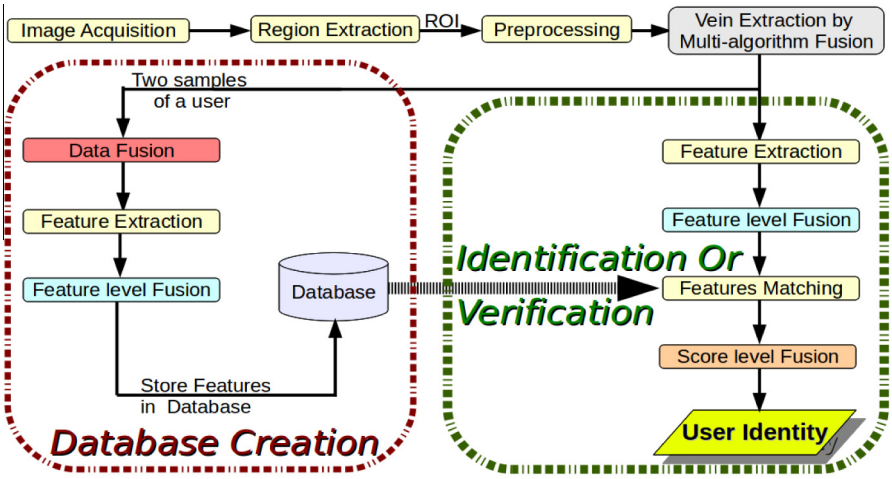

Fig. 1. Flow-graph of proposed system.

3. a metal rod with endpoints joined with center of side walls of box and is grasped by user hand such that palm-dorsa part of user is exposed to SLR camera,
4. a fixed stand to hold the system static while capturing images,
5. curtains to close the system to have low interference due to environmental conditions,
6. black colored walls of system and metal rod to distinguish hand with background easily,
7. several fixed parameters (like distance between camera and lamp, length of metallic rod, camera parameters and lamp positioning) to guarantee uniformity in acquisition procedure.

Fig. 2 shows the photograph of the acquisition system. Circular movements across metallic rod and elastic deformation in skin can introduce small non-linear deformation in the acquired image. Along with this, curved hand surface and lamp placement can result in non-uniform illumination and noisy background. Besides this, hair and some texture may also be present in images due to IR imaging. This is illustrated in Fig. 3. It shows background noise and hair in yellow and white bounding boxes respectively.

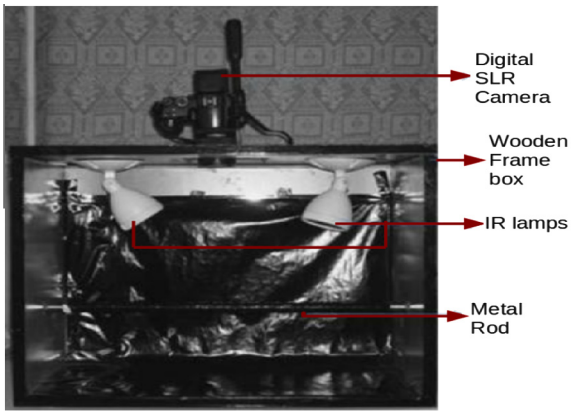

Fig. 2. Acquisition setup.

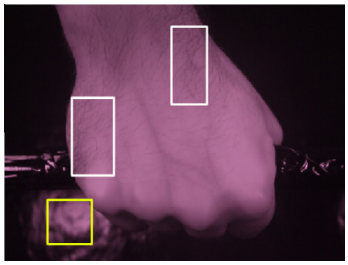

Fig. 3. A vein image with background noises and hairs.

3.1.2. Region extraction and preprocessing

Algorithm 1. REGION EXTRACTION AND PREPROCESSING($I_{original}$)

Require: Acquired palm-dorsa image, $I_{original}$.

Ensure: I_1^{enh} stores the enhanced palm-dorsa image.

1: Down-sample $I_{original}$ and convert to gray scale to generate image X.
2: Speckles are removed from X using median filter. Let I denotes the filtered image.
3: Skin pixels are detected from I using global thresholding [33]. Let $\hat{I}$ denotes the binarized containing 1 for skin pixels and 0 otherwise.
4: Some spurious skin pixels are generated due to noise. These are removed by erosion operation.
5: Connected components in $\hat{I}$ are detected using 8-neighborhood connectivity.
6: Among these, the component containing the maximum area represents the palm-dorsa area. Let the maximum area component be denoted by C_{max}^{A}.
7: Locations of the pixels containing palm-dorsa area is determined by the pixels forming C_{max}^{A}. The palm-dorsa area present in I is extracted using the locations and let it be I_{ROI}.
8: CLAHE [34] is applied on I_{ROI} to improve the contrast. Let the resultant enhanced image be $\bar{I}$.
9: Locations of hair are detected by applying Laplacian of Gaussian on $\bar{I}$ because hair contains sharp edge. Such pixels are stored in X.
10: Hairs are removed from $\bar{I}$ by applying mean filter at noise pixels stored in X. Let I_1^{enh} denote the resultant image.
11: **return** (I_1^{enh})

Since acquired image, I has a large size (3488×2616), it is down-sampled to 1/4th of its actual size and converted to gray scale. Median filter is used to remove the speckles [35]. As compared to other pixels, intensity values of skin pixels or foreground pixels are highly discriminating. Hence, global thresholding [33] can be used to detect foreground pixels. Spurious foreground pixels generated due to noise are removed by morphological operations [36]. Neighborhood connectivity [37] on foreground pixels is used to detect all components. Since palm-dorsa occupies the largest foreground area in the acquired image, the component having maximum area is marked as foreground and the remaining components are marked as background. All the background pixels in I are suppressed to obtain the ROI [38]. Contrast limited adaptive histogram equalization (CLAHE) [34] is applied on ROI to obtain the preprocessed image, $\bar{I}$. It improves the contrast but it may have the noise due to hair or texture which needs to be removed. It is observed that such noise has sharp edges as compared to vein pattern which contains smooth blurred edges. Thus, a Laplacian of Gaussian (LOG) filter [39] can be applied to detect the noise caused due to hair. Mean filter at the locations of hair has been used to eliminate such type of noise which is subsequently minimized by mean filter. Let such an enhanced image be referred as I_1^{enh}. An example of I_1^{enh} is shown in Fig. 4. Steps involved in ROI extraction and preprocessing are described in Algorithm 1.

3.1.3. Multi-algorithm fusion for veins extraction

Since global and local threshold based algorithms cannot extract the vein pattern accurately, a fusion algorithm is proposed in this section. The multi-algorithm fusion algorithm extracts the vein pattern from I_1^{enh} by fusing the outcomes of a global and a local threshold based algorithms. Flow-graph of the extraction of vein pattern from the enhanced image I_1^{enh} is shown in Fig. 5. Since I_1^{enh} contains low local contrast and non-uniform illumination which can interfere in vein extraction, it is first enhanced.

Vein patterns have variable width which generally look like Gaussian in cross sectional profile while line in the tangential direction [40]. Thus, a vein shaped matched filter proposed in [41] is applied at multiple scales [42] to enhance the variable width veins and to suppress the additional noise, if any. Such a filter, $g_{\phi,\mathbf{s}}(\mathbf{x},\mathbf{y})$ at location $(\mathbf{x},\mathbf{y})$ and scale $\mathbf{s}$ is given by

$$g_{\phi,\mathbf{s}}(\mathbf{x},\mathbf{y}) = -e^{-\left(\mathbf{a}^2/\mathbf{s}\sigma^2\right)}$$

where σ is the standard deviation used to define the Gaussian shape in cross sectional profile; ϕ is the direction of the filter; and $\mathbf{a}$ is given by

$$\mathbf{a} = \mathbf{x}cos\phi + \mathbf{y}sin\phi \qquad |\mathbf{a}| \leqslant 3\mathbf{s}\sigma$$

such that

$$\mathbf{b} = \mathbf{y}cos\phi - \mathbf{x}sin\phi \qquad |\mathbf{y}'| \leqslant \mathbf{s}\beta/2$$

where β is the length of line in tangential direction. Filter, $g_{\phi,\mathbf{s}}$ is normalized to zero mean using

$$g_{\phi,\mathbf{s}}(\mathbf{x},\mathbf{y}) = g_{\phi,\mathbf{s}}(\mathbf{x},\mathbf{y}) - mean\left(g_{\phi,\mathbf{s}}(\mathbf{x},\mathbf{y})\right)$$

The filter response of I_1^{enh} at scale $\mathbf{s}$ is given by

$$R_g^s(\mathbf{x},\mathbf{y}) = g_{\phi,\mathbf{s}}(\mathbf{x},\mathbf{y}) \circledast I_1^{enh}(\mathbf{x},\mathbf{y}) \tag{1}$$

where $\circledast$ represents convolution operator [43]. Similarly, filter responses at two different scales, $\mathbf{s_1}$ and $\mathbf{s_2}$ are evaluated using Eq. (1). Both filter responses are consolidated by element-wise product [44] to obtain the vein enhanced image, I_2^{enh}. That is,

$$I_2^{enh}(\mathbf{x},\mathbf{y}) = R_g^{\mathbf{s_1}}(\mathbf{x},\mathbf{y}) * R_g^{\mathbf{s_2}}(\mathbf{x},\mathbf{y})$$

where $*$ represents element-wise product. Boundary of palm-dorsa is also enhanced along-with vein pattern during matched filtering which can be removed by using palm-dorsa boundary and morphological operations [45].

Algorithm 2. MULTI-ALGORITHM FUSION FOR VEIN EXTRACTION(I_1^{enh}, G_1, G_2)

Require: Enhanced ROI image, I_1^{enh} and matched filters G_1 and G_2.
Ensure: Binary image I_F containing 1 at vein position otherwise 0.

1: //Apply multi-scale matched filter for vein enhancement and removing the hand boundaries.
2: $R_g^{s_1} = G_1 \circledast I_1^{enh}$ //$\circledast$ is the convolution filter.
3: $R_g^{s_2} = G_2 \circledast I_1^{enh}$ //$R_g^{s_1}$ and $R_g^{s_2}$ are filter responses.
4: $M = \left(R_g^{s_1} * R_g^{s_2}\right)$ //pixel-wise multiplication.
5: Boundary of th palm-dorsa is obtained by applying canny edge detector on I_1^{enh}. Let B_l contains the detected boundary.
6: B_l is dilated and the dilated image is subsequently removed from M to obtain I_2^{enh}.
7: //Vein extraction.
8: Local normalization is applied on I_2^{enh} followed by thresholding [33] to handle the problem of non-uniform illumination. Let the resultant image be A.
9: Evaluate $F(\mathbf{x},\mathbf{y}) = \frac{I_2^{enh}(\mathbf{x},\mathbf{y})}{I_1^{enh}(\mathbf{x},\mathbf{y}) + \epsilon}$ for each pixel $(\mathbf{x},\mathbf{y})$.
10: F contains high value at vein pixels and low values at other parts. Vein pixels in F are detected by using global thresholding. Let the vein pixels are stored in $\bar{B}$.
11: Neighborhood connectivity and threshold on area are used to remove noise components and its result is stored in B.
12: Images A and B are fused using binary OR operation. Let the fused image be I_f.
13: Neighborhood connectivity and threshold on area are used to remove noise components from I_f and its result is stored in I_F.
14: **return** (I_F)

It has been observed that local thresholding may fail to extract veins because of the existence of noise. Also, global thresholding may not provide good results when there are low intensities near actual vein but high intensities near noise areas. Thus, we have fused the results of local and global thresholding to extract the veins. Since I_2^{enh} suffers from the problem of non-uniform illumination, local normalization [46] followed by thresholding is applied on I_2^{enh} to obtain the binarized image A_L. It contains vein pattern and some noise as a foreground. Again, images I_1^{enh} and I_2^{enh} have low and high intensities respectively for vein pattern. An image F having high values at vein pattern and low values at other parts is formed by

$$F = \frac{I_2^{enh}}{I_1^{enh} + \epsilon} \tag{2}$$

where ϵ is a small constant. Global thresholding is applied on F to obtain $\bar{B}$ which may contain background noise. Background noise can be removed by using neighborhood connectivity and threshold on the detected component area [47]. Let resultant image be A_G. It is

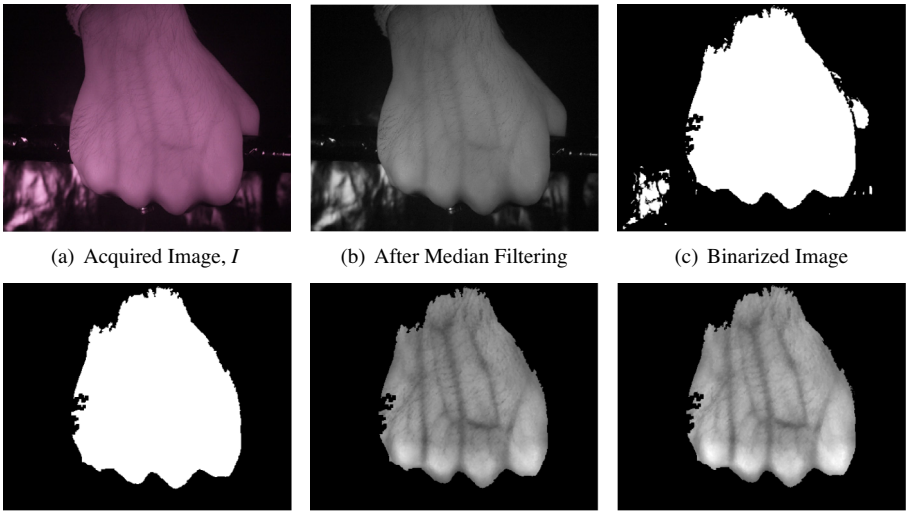

(a) Acquired Image, I (b) After Median Filtering (c) Binarized Image

(d) Palm-dorsa Area (e) CLAHE enhancement, $\bar{I}$ (f) After Noise Removal, I_1^{enh}

Fig. 4. Results of region extraction and preprocessing.

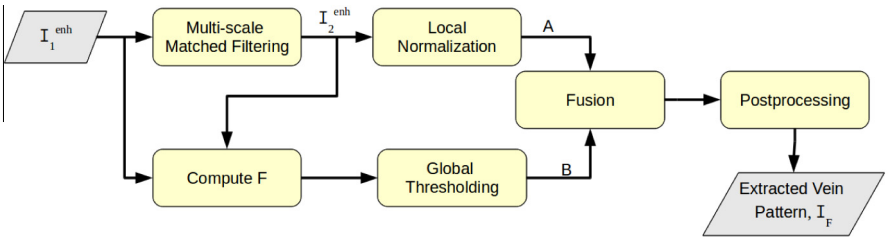

Fig. 5. Various stages of vein extraction.

observed that some vein areas are present in A_L and some in A_G. Thus, A_L and A_G are fused to obtain vein pattern by binary OR. Let I_f represents the fused image. It contains background noise which are removed by neighbor connectivity and threshold on the area. In addition, morphological closing operation is applied on it to remove the holes, if any. Let I_F denotes the resultant image which contains the genuine vein pattern. Fig. 6 shows resultant images A_L, A_G and I_F of the image shown in Fig. 4(a). Steps involved in vein extraction from the enhanced palm-dorsa image, are given in Algorithm 2.

3.2. Data fusion

Non-uniform illumination or hair can generate false veins or false cavities in the extracted vein pattern. A cavity is the small background (containing 0's) area in a vein. False veins or false cavities can result in false feature extraction and thus, wrong matching results. To illustrate, consider Fig. 7(a) and (b) where false veins, spurious cavities and genuine cavities are shown in blue, red and green colored circles respectively. Two vein patterns of the same hand have been fused to eliminate these false veins or false cavities. It is done during data enrollment to avoid the high computational cost and non-availability of multiple samples during authentication/verification process.

Let S_1 and S_2 represent the extracted binary vein patterns corresponding to a hand. These images are first registered by using image registration algorithm proposed in [49] to handle the non-linear deformation. Let V_1 and V_2 be the registered image corresponding to S_1 and S_2 respectively. Since it is more likely that a false vein is absent in one of the two samples, binary AND operation is applied on V_1 and V_2 to remove false veins. Let I_{fused} represent the resultant image. Unfortunately, if a spurious cavity (containing 0's) is present in either V_1 or V_2, then it is also present in I_{fused} due to AND operation. To obtain genuine vein pattern, such spurious cavity should be removed from the resultant image I_{fused}. The following observations help to determine whether a cavity is spurious or not:

1. A genuine or spurious cavity belongs to the background of an image and has small area. Thus, it belongs to the foreground in the negative of the image.
2. A spurious cavity belongs to the background (containing 0's) in exactly one of the two image, V_1 and V_2.
3. A genuine cavity belongs to the background (containing 0's) in both the images, V_1 and V_2.

To detect the cavities, foreground components present in the negative of the image can be determined by applying 8-neighborhood connectivity. Further, each cavity has small area. Thus, threshold on the area of these foreground components is subsequently used to detect each cavities in the image. These detected cavities are either spurious or genuine cavities. For classification, binary OR operation is applied on V_1 and V_2 at the locations of the cavities. If there are several 1's in the resultant area then the

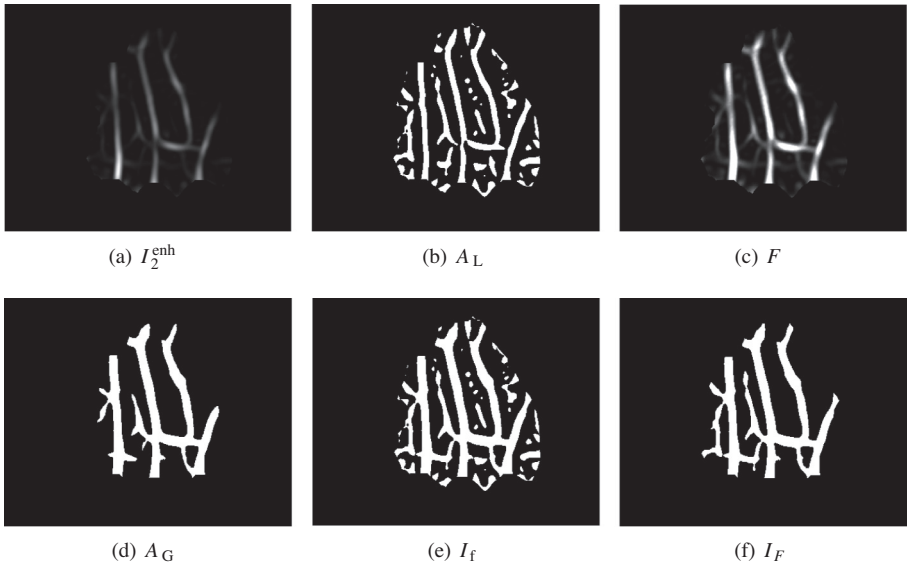

(a) I_2^{enh} (b) A_L (c) F

(d) A_G (e) I_f (f) I_F

Fig. 6. Vein extraction for Fig. 4(a).

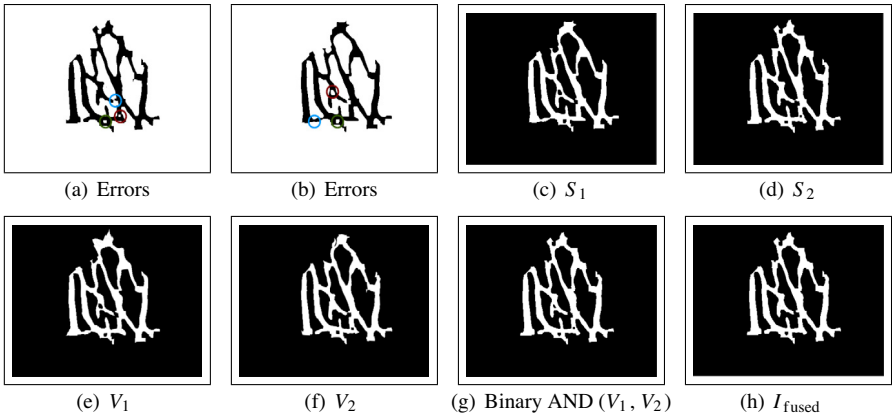

(a) Errors (b) Errors (c) S_1 (d) S_2

(e) V_1 (f) V_2 (g) Binary AND (V_1, V_2) (h) I_{fused}

Fig. 7. Various stages for data fusion.

cavity is spurious otherwise the cavity is genuine. Detected spurious cavities are removed from the image by marking these as foreground. The proposed data fusion simultaneously removes the false veins and spurious cavities while keeping the genuine vein pattern intact. Example of data fusion is shown in Fig. 7. Spurious false veins and spurious cavities present in S_1 and S_2 are removed in Fig. 7(h).

3.3. Feature extraction

In this section, different type of features is extracted from the given palm-dorsa image. Let C be the extracted vein pattern, i.e., either I_F in case of authentication/verification or I_{fused} in case of enrollment. Bifurcation of vein pattern and boundary of palm-dorsa have been used along-with vein shape to design the system.

3.3.1. Extraction of minutiae features

In this section, bifurcations and endings of vein pattern are extracted. It is observed that vein endings are not much discriminating and usually these are spuriously generated. Hence, bifurcations can be used as features while endings can be considered to remove spurious bifurcations. Algorithm [50] is applied on C to extract the skeleton, S. It may be spuriously disconnected. To connect these, S is dilated and subsequently its skeleton, S_1, is obtained. Line fitting [51] has been applied on S_1 to remove hair like structure near vein endings, if present. Let resultant image is given by S_F. Endings and bifurcations are extracted from S_F by using [20]. Some bifurcations may be spurious as can be seen inside the blue bounding box of Fig. 8(e). Such spurious bifurcations can be removed using the fact that the Euclidean distance between an ending and a bifurcation point should not lie within some range. Let B stores the location of true bifurcations. Consider Fig. 8 for better understanding of the proposed bifurcation extraction. Some spurious disconnections are shown in red bounding box of Fig. 8(b). These are removed after morphological operations as shown in Fig. 8(c). An example of hair like structure is shown inside green bounding boxes. These are removed after line fitting which is shown in Fig. 8(d). Fig. 8(e) shows the extracted bifurcations (in green) and endings (in red), while Fig. 8(f) shows only genuine bifurcations on S_F. The steps required to obtain B from the extracted vein pattern, are given in Algorithm 3.

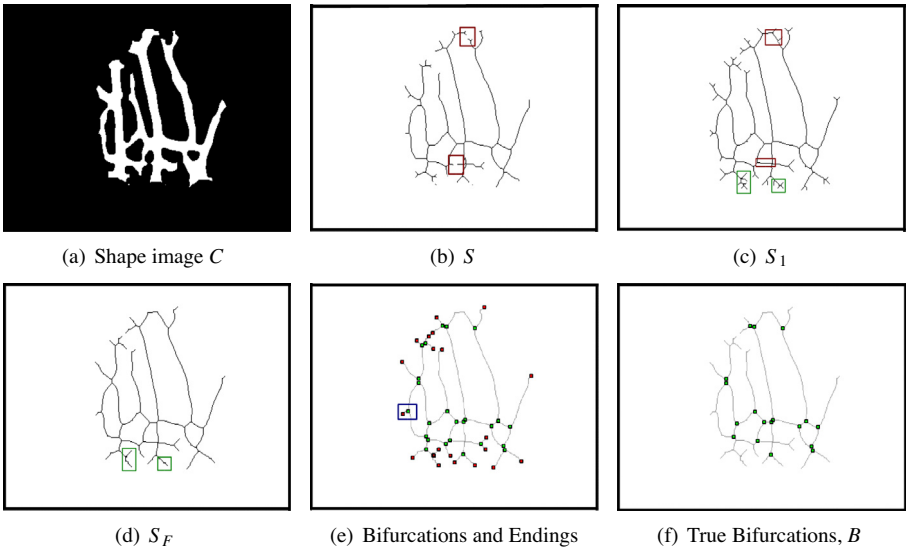

(a) Shape image C (b) S (c) S_1

(d) S_F (e) Bifurcations and Endings (f) True Bifurcations, B

Fig. 8. Minutiae feature extraction.

Algorithm 3. MINUTIAE REPRESENTATION(I)

Require: Extracted vein pattern, I.
Ensure: Return B which stores true bifurcations.
1: Skeleton of I is detected and stored in S.
2: S may be spuriously disconnected, which is reconnected by applying dilation operation on S. Find skeleton of the dilated image and denote it as S_1.
3: Hair like structure near vein endings are removed by smoothing S_1 using line fitting. Let the resultant image be S_F.
4: /*Let **E** and **B** store location of extracted endings and bifurcations respectively.*/
5: Bifurcations and endings are extracted from S_F and store these in $(\mathbf{E}, \mathbf{B})$.
6: Spurious bifurcations are detected from **B** by using the fact that the Euclidean distance between an ending and a bifurcation point should not lie within some range. Let spurious bifurcations be **A**.
7: $\mathbf{B} = \mathbf{B} - \mathbf{A}$ //removing spurious bifurcations.
8: **return** (B)

3.3.2. Extraction of boundary features

Boundary of palm-dorsa, $B_{\widehat{I}}$, is obtained by applying canny edge detector on the palm-dorsa image, I_1^{enh}. It is observed that some part of palm-dorsa boundary which contains joints are stable in nature due to bones and hand placement on the metal rod. It is given by the part of palm-dorsa boundary which lie below the metallic rod in the acquired image. This part mainly concentrates on the shape of knuckles. Let the lower position of the rod in the acquisition setup is given by line B_P. Therefore, all the boundary pixels above B_P are removed to obtain new boundary, D_j. Deformations due to the elastic nature of the skin in D_j are handled by dilation. The dilated image, B_J, is used as boundary feature. An example of boundary feature extraction is shown in Fig. 9.

3.4. Feature level fusion

Shape based methods are found to be highly useful for vein pattern recognition. Its usefulness can be further increased if other features representing the local behavior are also used. Thus, feature level fusion of shape (C) and bifurcations is carried out.

Algorithm 4. FEATURE LEVEL FUSION(B, C)

Require: B and C which store true bifurcations and shape of vein respectively.
Ensure: Return I_{ff} which stores the feature fused image.
1: Image S_M is created such that S_M and I have same dimensions.
2: $S_M = 0$ //S_M has zero intensity at each pixel
3: Let **Z** contains the number of true bifurcations in B.
4: **for i** $= 1$ to **Z** **do**
5: /* Let (x_i, y_i) be the location of $\mathbf{i_{th}}$ genuine bifurcation stored in **B**. */
6: **for** each pixel $(\mathbf{x}, \mathbf{y})$ in S_M **do**
7: $S_M(\mathbf{x},\mathbf{y}) = S_M(\mathbf{x},\mathbf{y}) + \sum_{i=1}^{Z} \frac{1}{2\pi\sigma_m^2} \times e^{\left(-\frac{(\mathbf{x}-\mathbf{x_i})^2+(\mathbf{y}-\mathbf{y_i})^2}{2\sigma_m^2}\right)}$
8: **end for**
9: **endfor**
10: **for** each pixel $(\mathbf{x}, \mathbf{y})$ in S_M **do**
11: $I_{ff}(\mathbf{x},\mathbf{y}) = S_M(\mathbf{x},\mathbf{y}) + C(\mathbf{x},\mathbf{y})$
12: **end for**
13: **return** (I_{ff})

All probable locations of true bifurcations are initially stored in the form of an image, S_M. Intensity at each pixel $(\mathbf{x}, \mathbf{y})$ in S_M is given by

$$S_M(\mathbf{x},\mathbf{y}) = \sum_{i=1}^{Z} \frac{1}{2\pi\sigma_m^2} \times e^{\left(-\frac{(\mathbf{x}-\mathbf{x_i})^2+(\mathbf{y}-\mathbf{y_i})^2}{2\sigma_m^2}\right)} \quad (3)$$

where **Z** is the number of true bifurcations; σ_m is the standard deviation; and $(\mathbf{x_i}, \mathbf{y_i})$ represents the location of $\mathbf{i^{th}}$ true bifurcation. Feature fused image, I_{ff}, is obtained by pixel-wise addition of C and S_M. Example of feature level fusion is shown in Fig. 10. Steps involved in feature level fusion are discussed in Algorithm 4.

3.5. Feature matching

Boundary feature image, B_J and feature fused image, I_{ff} of the probe palm-dorsa image, I, are matched with the stored feature

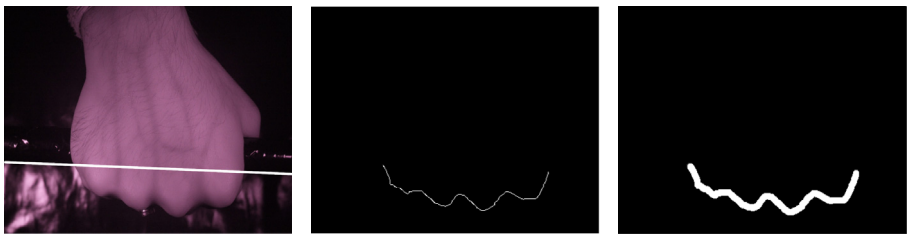

(a) $I_{original}$ overlay with B_P (b) D_j (c) B_J

Fig. 9. Boundary feature extraction.

(a) Shape image C (b) S_M for Figure 8(f) (c) I_{ff}

Fig. 10. Feature level fusion.

images. Let G represent the gallery palm-dorsa image whose boundary image and feature fused image are given by B_J^G and I_{ff}^G respectively. For matching I_{ff} and I_{ff}^G, global matching based on phase correlation matching is used because it can handle the missing of few genuine veins and generation of few spurious veins. Frequency responses of I_{ff} and I_{ff}^G obtained by using fast fourier transform (FFT), are used to find cross-power spectrum whose inverse FFT gives correlation image, C_M^I. Each pixel in C_M^I represents the matching score of I_{ff}^G and I_{ff} when I_{ff} has undergone some translation changes [52]. Steps involved in obtaining the correlation image are described in Algorithm 5. Similarly, correlation image C_m^B of B_J^G and B_J^P is obtained.

Algorithm 5. POC(I_1, I_2)

Require: Two images I_1 and I_2
Ensure: Correlation image or matching score for all possible translations, C_M
1: $I_1^F = \text{FFT}(I_1)$ //FFT represent fast fourier transform.
2: $I_2^F = \text{FFT}(I_2)$
3: $I_2^F = \text{CONJUGATE}\left(I_2^F\right)$
4: /* C_M^F represents cross-power spectrum */
5: $C_M^F = \frac{(I_1^F) \circledast (I_2^F)}{|I_1^F I_2^F|}$
6: $C_M = \text{IFFT}\left(C_M^F\right)$
7: **return** (C_M)

3.6. Score level fusion

Correlation images C_m^I and C_m^B are fused to obtain the matching score of P and G. Intuition behind the proposed fusion is that for a particular translation parameter, matching scores of fused feature image and boundary feature image are high in the case of genuine matching. Thus, product fusion of matching scores at possible translations are calculated and maximum among them is considered as the matching score of P and G. Mathematically, product fusion of correlation images C_m^I and C_m^B at possible translation is given by

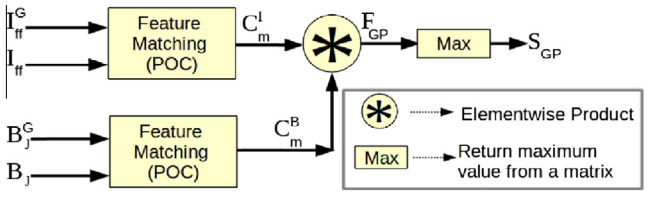

Fig. 11. Feature matching and score level fusion.

$$F_{GP}(\mathbf{x},\mathbf{y}) = C_m^I(\mathbf{x},\mathbf{y}) \times C_m^B(\mathbf{x},\mathbf{y}) \tag{4}$$

where $(\mathbf{x},\mathbf{y})$ represents a pixel location and F_{GP} stores the fused results for all possible translations. Eventually, matching score between G and P is given by

$$S_{GP}(P,G) = max((F_{GP}(\mathbf{x},\mathbf{y}))\forall(\mathbf{x},\mathbf{y})) \tag{5}$$

Flow-graph used to obtain the matching scores of G and P from the feature fused images and boundary images is shown in Fig. 11.

4. Experimental results

The performance of the proposed system is assessed by conducting the experiments on IITK database which consists of 4120 images acquired from 1030 users. It has 4 samples for each user. Two images of each user are placed in a gallery set while the rest are kept in probe set. All these systems required in the experimentation are simulated on a computer having Intel Pentium 8 processor, 2.8 GHz with 4 GB RAM. Also, these are implemented in MATLAB 7.2.

Decision of match/unmatch is taken based on threshold, t, in case of verification. If the matching score, S_{GP}, is greater than t, then it indicates a match; otherwise it is unmatch. Therefore, false accept rate (FAR) and false reject rate (FRR) are the defined in

terms of t. A receiver operating characteristic (ROC) curve can be used to see the behavior of FAR and FRR at different threshold values. Equal error rate (EER) is used as evaluation metrics for verification at a confidence measure (CI) for 90% interval [53]. EER is given by the false accept rate at a particular threshold t_1, such that FAR(t_1) = FRR(t_1). The proposed system has achieved an EER of 1.418e–4% at CI of 1.3468e–04%. Its receiver operating characteristic (ROC) curve is given in Fig. 12. Also, correct recognition rate (CRR) is used to measure the performance of the system for identification. It is the accuracy for the top best match, which is given by:

$$\mathrm{CRR} = \frac{\text{Total number of correct top match}}{\text{Total number of query images}} \times 100 \tag{6}$$

CRR of the proposed system is found to be 100%. Fig. 13 shows the distance between the genuine score and the nearest impostor score for each user. Clear separation between impostor scores and genuine scores is visible in it.

4.1. Parameter tuning

There are several parameters used in the proposed system to generate accurate results. Impact and tuning of these parameters are discussed below:

1. **Parameters used in the preprocessing stage**: Preprocessing of the acquired image containing only palm-dorsa area requires a LOG filter to detect hair and mean filter is used to remove the detected hair from the image. These filters depend based on the noise characteristics. LOG filter is designed using two parameters, viz., (i) standard deviation, σ_l, of the Gaussian filter that is required for smoothing; and (ii) kernel size of the Laplacian filter that is useful for detecting the edges or high frequency components. Suitable selection of σ_l plays an important role in hair detection. If a large value of σ_l is used, then hair may not be visible because high frequency components from hair are blurred out. In contrast, if small value of σ_l is used, then even vein pixels containing small intensity variation can also be detected as hair. To detect the hair and smoothen the vein pixels, σ_l is chosen such that the Gaussian filter used in LOG closely resembles the shape of hair [54]. In our experiment, twice of σ_l is considered as the average width of hair. It is approximately 3 pixels. Thus, σ_l is set as 1.5. In addition, kernel size of the Laplacian filter in each dimension is given by $3 \times \sigma_l$, round to the nearest odd integer. That is, its size is 5×5. By this, borders of the Laplacian filter reach nearly to zero and thus, sometime discontinuities in the filtered image can be avoided [55]. Similarly, in this paper, detected hair are removed by a mean filter. Assume that its size is $2w_m + 1$ in each dimension. It is designed using the intuitions used in [55]: (i) w_m should be greater than the diameter of the noise, which is the average width of hair (approximately 3 pixels) in our case; and (ii) w_m should be small to avoid minimize computational time and large smoothing. Hence, a mean filter of size 7×7 is used.
2. **Parameters used in the veins extraction stage**: In the stage of multi-algorithm fusion for vein extraction, multi-scale matched filtering is applied to vein enhancement. An accurate vein enhancement requires careful selection of various parameters. Parameters required in matched filtering are standard deviation σ, length β and direction ϕ of the matched filter. For accurate results, parameters of matched filtering should be selected in such a way that the filter shape and the feature shape should closely resemble to each other [56]. Clearly, visible thick veins are manually marked in 25 randomly selected palm-dorsa images. In cross sectional profile, the average width of the marked veins is approximately 16. To approximate the shape of Gaussian in cross-sectional profile, σ is set to half of the average width of the marked veins, i.e., 8. If the small value of σ is used, then noise due to texture and hair can be enhanced, i.e., behave as veins. On the other hand, if the large value of σ is used, then genuine vein can be smoothen and thus, can be absent in the enhanced pattern. β is set to 16, i.e., size of matched filter is 16×16. If a large value of β is assigned, then the vein area containing large curvature cannot be accurately detected. In contrast, sometime pixels containing Gaussian noise can be detected as vein pixels if small value of β is used. Also, parameter ϕ is set equal to 90° because most of the veins are in vertical direction. The proposed system uses multi-scale analysis for enhancing both thick and thin veins. It is observed that the average width of thin veins is approximately half of the average width of thick veins. Thus, $\mathbf{s_1}$ is set to 1 for enhancing thick veins while $\mathbf{s_2}$ is set to $\frac{1}{2}$ for enhancing thin veins.
3. **Parameters used in the data fusion stage**: A threshold is used to detect the cavities present the vein pattern. Let t_a^c denote the threshold. Cavities are usually formed at the locations where several veins can intersect. Shape at these locations looks like neither a Gaussian in cross sectional profile nor a line shape in the tangential direction. Thus, vein enhancement using matched filtering fails to enhance the veins present at these locations. If low value of t_a^c is used, then genuine cavity can be missed. In contrast, large spurious cavities can be generated if the large value of t_a^c is used. It is set to be the maximum area such that the intersection of several veins can attain. It is seen from the extracted veins that at most four veins can intersect in a close proximity and the average width of the veins in our case is approximately 16. Thus, t_a^c is set to $4 \times 16 \times 16$.
4. **Parameters used in the feature level fusion**: Parameter σ_m in Eq. (3) is the standard deviation. It has been observed that the actual location of a minutiae can be deviated due to skeletonization. If small value of σ_m is used, then genuine matched minutiae pair can be missed due to deviation introduced by skeletonization. And if the large value of σ_m is used, then spurious minutiae pairs can be matched. In this paper, twice of σ_m is set to the average width of the veins, i.e., 16.

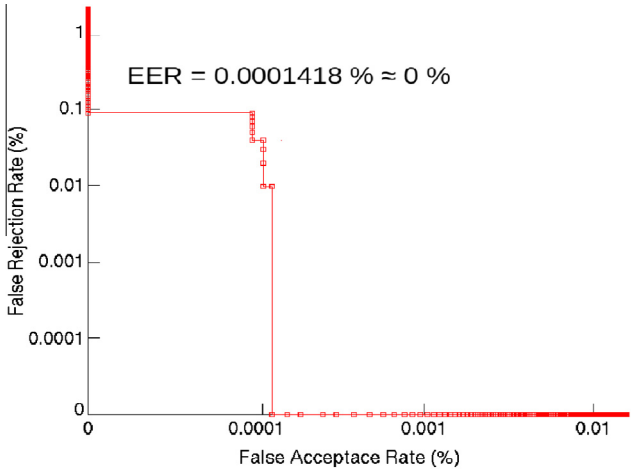

Fig. 12. ROC of the proposed system.

4.2. Performance of vein extraction

The importance of the proposed vein extraction is shown in Table 1. All the experiments presented in Table 1, are performed under same conditions. It considers only contour features which

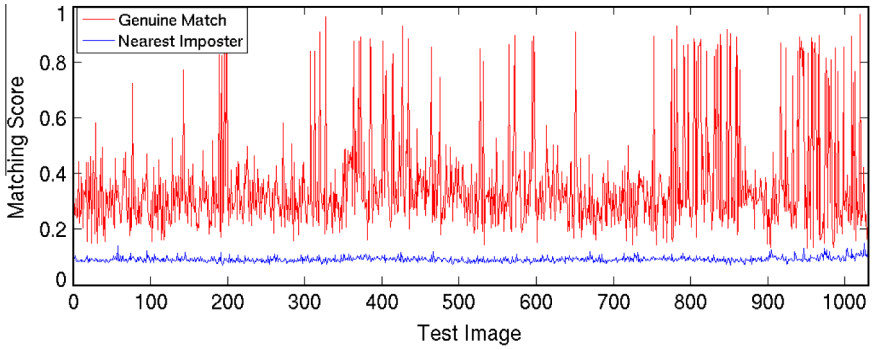

Fig. 13. Genuine and nearest imposter matching scores.

Table 1
Results for vein pattern extraction in EER (%).

	Vein extraction algorithm	Local	Global	Fusion
[10]	Gabor filtering	8.73	7.16	5.27
[9]	Steerable filtering	9.05	7.84	5.36
[14]	Line tracking + maximum curvature	14.26	13.81	10.12
$\bar{I}$	Multi-scale matched filtering	9.37	5.52	1.38
I_1^{enh}	Multi-scale matched filtering	6.14	3.65	**0.13**

Bold indicates the results obtained by the proposed algorithm.

are matched by using the proposed feature matching. Vein extraction mainly consists of preprocessing of ROI, vein enhancement and vein extraction. ROI enhanced image, I_1^{enh} is obtained by applying hair and texture removal preprocessing on $\bar{I}$. Thus, $\bar{I}$ is used instead of I_1^{enh} in Table 1 to show the importance of removal of hair and texture. Similarly, enhanced palm-dorsa images are used instead of I_1^{enh} to analyze their performance. In addition, veins are extracted from the enhanced images by using local thresholding, global thresholding and their proposed multi-algorithm fusion. It is evident from Table 1 that (i) vein extraction by multi-scale matched filtering performs better than other well known systems; (ii) multi-algorithm fusion performs better than local and global thresholding; (iii) performance can be improved if noise due to hair or texture can be removed; and (iv) the proposed vein extraction shows better results than any other combination.

4.3. Performance of minutiae extraction

It has been observed that minutiae endings are not much discriminating and often these are spuriously generated. Also, skeletonization plays a crucial role in the accurate minutiae extraction; thus, it should be accurate. Therefore, the performance of the proposed system in terms of minutiae features and skeletonization is analyzed with the help of Table 2. Experiments shown in Table 2, are performed under same conditions. In case of minutiae based matching, a vein pattern must contain a large number of minutiae for accurate vein pattern recognition. But it is not always feasible as can be observed from Fig. 14 which shows the distribution of extracted minutiae bifurcation on IITK database. In Fig. 14, there are 235 vein images which contain less than 7 minutiae bifurcations that can be generated due to missing of genuine

Table 2
Impact of minutiae endings and bifurcations on performance.

	S	S_1	S_F
Endings	11.73	10.97	7.46
Bifurcations + endings	9.87	8.92	5.73
Bifurcations	1.84	1.86	**0.4**

Bold indicates the results obtained by the proposed algorithm.

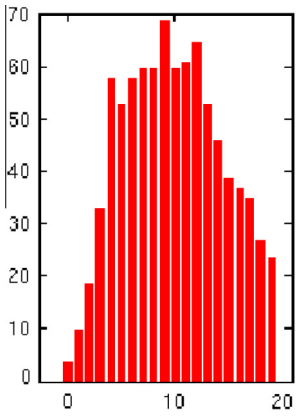

Fig. 14. Distribution of minutiae bifurcations.

veins. Only minutiae features are matched by using the proposed feature matching. It considers the vein images having more than 7 minutiae bifurcations. Its results are evaluated by using minutiae endings and bifurcations extracted from different skeleton images, viz., S, S_1 and S_F. Table 2 indicates that:

1. S_F has better performance than S and S_1, which indicates that most of the spurious minutiae are absent in S_F.
2. The performance of the system degrades as the use of minutiae endings increases. It suggests that most of the obtained minutiae endings are spurious in nature.
3. The proposed bifurcation based system performs better than other combinations.

4.4. Performance of fusion strategies

Table 3 shows the effectiveness of various fusion strategies. It uses the following feature representations: (i) contour (C), (ii) minutiae representation (S_M), and (iii) boundary (B_J). Its initial three tests use only one feature. In other tests, multiple features are used along with different fusion strategies. Data fusion is carried out in every test. All the tests in Table 3 are performed under same conditions. Feature level fusion is used in Test 4, Test 6, Test 8 and Test 10 and it refers to the pixel-wise addition of different features. Similarly, score level fusion is done in Test 5, Test 7, Test 9 and Test 10 by Eqs. (4) and (5). Some observations that can be derived from Table 3 are as follows:

1. It is apparent from every test that the performance is improved by using data fusion. It is because some spurious bifurcations, spurious cavities and spurious vein are removed by data fusion.

Table 3
Usefulness of various feature extraction and fusion strategies.

Test	Features used	Feature fusion	Score fusion	Data fusion	EER	Confidence
1	C	X	X	X	0.1312	0.1047
				✓	0.1289	0.0937
2	S_M	X	X	X	32.1857	1.3235
				✓	28.5164	1.1938
3	B_J	X	X	X	36.5723	1.4523
				✓	36.5723	1.4523
4	$C + B_J$	✓	X	X	0.3524	0.4728
				✓	0.1768	0.1742
5	$C + B_J$	X	✓	X	0.1153	0.1403
				✓	0.0989	0.0820
6	$C + S_M$	✓	X	X	0.1043	0.0842
				✓	0.0963	0.0785
7	$C + S_M$	X	✓	X	16.6186	1.347
				✓	12.8241	1.239
8	$S_M + B_J$	✓	X	X	11.2841	0.849
				✓	9.4564	0.841
9	$S_M + B_J$	X	✓	X	10.2752	0.826
				✓	9.2752	0.718
10	$C + S_M + B_J$	✓	✓	X	9.571e−3	2.5271e−04
				✓	**1.418e−4**	**1.3468e−04**

Bold indicates the results obtained by the proposed algorithm.

2. System rely on only shape features (Test 1) performs better than those rely only on vein bifurcations or boundary features (Test 2 and Test 3). This is because of the fact that (i) boundary features are not very distinct and look very similar; and (ii) in some cases, there may not be a sufficient number of true vein bifurcations. But by fusing vein bifurcations, boundary and shape features in a proper way, performance can be increased.
3. It is observed from Test 4 and Test 5 that score level fusion is more appropriate than feature level fusion to fuse shape and boundary features. Also, score level fusion give better results as compared to the use of only shape or boundary features. This can be seen from the results of Test 5 against Test 1 and Test 3.
4. Likewise, score level fusion of boundary and bifurcations performs better than feature level fusion.
5. Feature level fusion is found to be better than score level fusion if one considers shape and vein bifurcations features for fusion. It is apparent from Test 6 and Test 7. Score level fusion mainly fails when there are less number of bifurcations.
6. The proposed system that uses all three levels of fusion gives the best result.

4.5. Comparative performance analysis

The competence of the proposed system as compared to other well known systems has been studied in Tables 4 and 5. It can be observed in Table 4 that the proposed system performs better than other known systems except the systems in [24,30] which have 0% EER. But systems in [24,30] have been tested on databases of size only 47 and 12 respectively. Therefore, the proposed system is efficient in person authentication. For better comparative analysis, several systems are implemented and tested on IITK database whose results are presented in Table 5. Experiments shown in Table 5, are performed under same conditions. It illustrates that the proposed system exhibits better performance than other established systems. Reasons for better performance are:

1. Vein patterns are free from hair and texture.
2. System [57] relies on the skeleton which is highly susceptible to noise and non-uniform illumination and thus, it gives spurious results.
3. It has been observed that the proposed system performs better than minutiae based systems, [24,26]. The reasons behind low performance are:
   (a) **Few extracted minutiae**: A minutiae based matching system requires sufficient number of minutiae for correct matching [60]. But it is not always possible to obtain in case of vein pattern, For example, there are 235 vein images in IITK database which contains less than 7 bifurcations in each image and these have poor recognition results.
   (b) **Minutiae endings**: It has been observed that minutiae endings are often spuriously generated which degrade the system performance.
   (c) **Spurious minutiae generation**: Spurious minutiae can be generated due to spurious skeleton, non-uniform illumination and noise.
4. System [57] has better performance than other systems except the proposed system. Reason behind this is that system [57] makes use of vein shape and correlation matching which can handle the problems of missing of genuine veins and generation of spurious veins to a large extend.

Table 4
Performance of various vein based biometric systems on different databases.

System in	Dataset*			FAR (%)	FRR (%)	EER (%)	CRR (%)
	Users	Samples	Total				
[29]	20	5	100	0	5	–	–
[19]	32	30	960	2.3	2.3	2.3	–
[30]	12	9	108	–	–	0	–
[21]	100	5	500	0	0.5	–	–
[27]	500 × 2	5	5000	0.03	7.84	0.695	99.88
[24]	47	3	141	–	–	0	–
[57]	150	10	1500	–	–	1.43	–
[22]	100	3	300	–	–	1.14	–
[58]	100	5	500	–	–	–	95.1
[28]	102 × 2	10	2040	–	–	9.12	90.88
[23]	122 × 2	3	732	–	–	1.63	–
[25]	122	6	732	–	–	1.35	–
	34	∼6	173	–	–	3.6	–
[26]	122	6	732	–	–	0.41	–
	34	∼6	173	–	–	0.15	–
[59]	200 × 2	10	4000	–	–	–	97.6
[31]	100	–	400	–	–	0.41	–
	68	–	204	–	–	0.15	–
Proposed	1030	4	4120	0	2.836e−4	1.418e−4	100

–: Not reported. *: On different dataset.

Table 5
Performance of various vein based biometric systems on IITK database.

System	Remarks		EER (%)	CRR (%)
	Feature extraction	Matching		
[30]	Skeleton	*LHD*	32.12	71.23
[24]	Minutiae	*MHD*	36.39	69.46
[26]	Spectral minutiae	Correlation	21.78	82.62
[56]	Shape by Gabor filter	Correlation	8.45	93.34
Proposed	Vein structure, minutiae and hand boundary	Correlation + fusion	**1.418e−4**	**100**

Bold indicates the results obtained by the proposed algorithm.

5. The proposed system shows superior performance than other state of the art systems and it is shown to be highly accurate in person authentication. In this, the use of appropriate fusion strategies along with different features plays a crucial role.

4.6. Computational time

The computational time of a biometric system is very important to understand its applicability in real world scenarios. It is observed that data fusion which is used during database creation takes the largest amount of time, which is 4000 ms. Since the database is created in off-line mode, it does not impact the verification or authentication time. In addition, the time taken in region extraction is about 603 ms which is mainly due to the two inevitable steps, viz., loading and down-sampling of palm-dorsa image. Shape feature (C) is extracted in 524 ms and most of its time is taken by local normalization. Skeletonization which is the major step for minutiae extraction requires about 247 ms. But a feature matching which includes phase only correlation matchings and score level fusion in the proposed system takes only 6.24 ms. Thus, the proposed system can be used as an online authentication system. Time required to authenticate a subject against γ subjects in the database is about $(1383.84 + 6.24 \times \gamma)$ ms. The performance of the system is increased by using various features, threshold algorithms and fusion strategies, but it also increases the computation time. Some systems like [26,57] have less computation time than the proposed system which are $(951.35 + 6.13 \times \gamma)$ ms and $(994.27 + 6.16 \times \gamma)$ ms respectively, for authenticating γ subjects. It can be observed that the time taken for feature matching by the proposed system, system [26] and system [57] are almost similar, which are 6.24 ms, 6.13 ms and 6.16 ms. Thus, there computational times are almost similar when large database is used. The total time taken by the proposed system for authentication/identification of a user using IITK database is 7811.04 ms.

4.7. Performance on a publicly available database

GDPSvein database [61] has been used for performance analysis. It is a publicly available palm-dorsa database containing 1020 acquired from 102 users and each of size 1392×1040 pixels. It has 10 samples of each user. Its acquisition setup uses a rod containing two pegs. The pegs are used for positional reference. During acquisition, the right hand of a user grasp the rod such that the first peg lies between ring and middle fingers while the second peg lies between index and middle fingers. User's hand is illuminated by LEDs and a video camera is used for acquisition. The LEDs and the camera are placed above the rod and pegs in such a way that the palm-dorsa area is completely exposed to the camera. For evaluation, two images of each user are placed in a gallery set while the rest are kept in probe set.

Table 6 shows the competence of the proposed system as compared to other well known systems on GDPSvein database. Just like Table 3, it uses the following feature representations for better analyses: (i) contour (C), (ii) minutiae representation (S_M), and (iii) boundary (B_J). It can be seen from Table 6 that the proposed system performs better than other well known systems. However, the performance of the system is decreased on the database when compared with the performance evaluation of IITK database. The reason behind this can be mainly attributed to the acquisition setup. IITK database contains good quality images from which large number of thick and thin veins can be extracted. In contrast, images in GDPSvein database have low quality images and thus, genuine veins can be missed. It is claimed in [57] that approximately 20% of the images in GDPSvein database have poor vein contrasts.

Table 6
Performance of various vein based biometric systems on the GDPSvein database.

System	Remarks		EER (%)	100-CRR (%)
	Feature extraction	Matching		
[30]	Skeleton	*LHD*	40.53	37.13
[24]	Minutiae	*MHD*	43.62	46.81
[26]	Spectral minutiae	Correlation	34.45	29.17
[56]	Shape by Gabor filter	Correlation	5.27	5.64
B_J	Hand boundary	Correlation	39.76	28.80
S_M	Minutiae	Correlation	34.19	25.12
C	Vein structure	Correlation	3.18	4.29
Proposed	Vein structure, minutiae and hand boundary	Correlation + uusion	**1.31**	**1.84**

Bold indicates the results obtained by the proposed algorithm.

4.8. Discussion

Acquisition setup presented in this paper, is careful designed to acquire the good quality images containing only palm-dorsa of the human hand. Camera used in the acquisition setup can acquire only a specific amount of area. If the human palm-dorsa lies outside the area then it cannot be completely acquired. This issue is resolved by placing pegs or handle in the acquisition setup which constrained the positioning of the human palm-dorsa. A cylindrical rod, instead of peg based acquisition setup [62] has been used to acquire the proposed boundary feature, i.e., the shape of the knuckles. Some acquisition setups like in [22], acquire full hand image and avoid pegs. It acquires poor quality images and require additional time expensive processing for palm-dorsa localization. In most of the existing setups, data are acquired by the low quality camera. It acquires poor quality and low resolution images in which most of the genuine vein are occluded and several spurious veins are generated due to hair and hand texture. In contrast, the proposed acquisition setup uses a high quality camera to acquire an image containing clearly visible thick and thin lines. Like any other setup, several parameters are fixed in it like length of metallic rod, camera properties, lamp positioning and distances between camera, lamp and rod.

A database containing palm-dorsa veins can be acquired in several other ways. When the proposed system is applied on another database, then following results can be possible:

1. Boundary feature (i.e., the shape of the knuckles) is absent in the acquired image due to which boundary features do not provide accurate results.
2. Likewise, few minutiae bifurcations are available due to poor quality of the images. Thus, minutiae bifurcation does not perform accurately. Minutiae endings with minutiae bifurcations may provide better results.
3. Similarly, accuracy of vein shape matching can be decreased due to bad quality.

It can be inferred that the proposed system requires some modification based on the database to achieve better accuracy. Like, boundary feature can be avoided for a database whose images do not contain boundary feature and some other parameters can be tuned according to the database. The proposed system correctly extracts the palm-dorsa veins and utilized the veins for accurate personal authentication.

5. Conclusions

This paper has proposed a system which can accurately extract the vein pattern from a palm-dorsa image and uses it for personal authentication. Region of interest has been extracted from the given palm-dorsa image which contains noise (like skin texture or hair), non-uniform illumination and low local contrast. Such problems have been handled in this paper. The genuine vein pattern has been extracted from this preprocessed image by a multi-algorithm fusion strategy. Effectiveness of the proposed fusion strategy has mainly resulted from the usage of both local and global thresholding. A data fusion strategy has been used to remove spurious veins and cavities, if they are present. It has generated a reliable vein pattern during enrollment. In the proposed system, three different feature representations, viz., (i) minutiae, (ii) shape feature, and (iii) hand boundary shape have been used. Full hand boundary shape is unstable due to the elastic nature of the skin thus, some stable part of hand boundary is extracted and it is fused with another features to achieve better performance. A novel hybrid fusion has been proposed in this paper for fusion of different features. Initially, minutiae and shape feature have been fused to obtain a feature fused image by using feature level fusion. The feature fused image has been fused with boundary features by using score level fusion. The proposed system can compensate geometrical deformations in a time efficient manner.

The proposed system has been tested on a database of 4120 images from 1030 subjects. It has achieved an accuracy of almost 100% in identification and verification. It has been compared with some well known systems and is found to be efficient on the large size database. Also, our experimental results have suggested to use boundary features and vein bifurcations, but not to consider vein ending features to achieve better performance.

Acknowledgment

Authors like to acknowledge the support provided by the Department of Information Technology, Government of India to carry out this research work. Authors are also thankful to the anonymous reviewers for their valuable suggestions to improve the quality of the paper.

References

[1] P. Gupta, P. Gupta, An efficient slap fingerprint segmentation and hand classification algorithm, Neurocomputing 142 (2014) 464–477. http://dx.doi.org/10.1016/j.neucom.2014.03.049.
[2] M. Shahin, A. Badawi, M. Kamel, Biometric authentication using fast correlation of near infrared hand vein patterns, Int. J. Biomed. Sci. 2 (3) (2007) 141–148.
[3] A.M. Joussen, Vascular plasticity–the role of the angiopoietins in modulating ocular angiogenesis, Graefe's Archive for Clinical and Exp. Ophthalmol. 239 (12) (2001) 972–975.
[4] P.J. Flynn, A.K. Jain, A.A. Ross, Handbook of Biometrics, Springer, 2008.
[5] C. Wilson, Vein Pattern Recognition: A Privacy-enhancing Biometric, CRC press, 2011.
[6] L. Wang, G. Leedham, S.-Y. Cho, Infrared imaging of hand vein patterns for biometric purposes, IET Comput. Vision 1 (3) (2007) 113–122.
[7] M. Soni, S. Gupta, M. Rao, P. Gupta, A new vein pattern-based verification system, Int. J. Comput. Sci. Inform. Security 8 (1) (2010) 58–63.
[8] B. Huang, Y. Dai, R. Li, D. Tang, W. Li, Finger-vein authentication based on wide line detector and pattern normalization, in: International Conference on Pattern Recognition, IEEE, 2010, pp. 1269–1272.
[9] J. Yang, X. Li, Efficient finger vein localization and recognition, in: International Conference on Pattern Recognition, IEEE, 2010, pp. 1148–1151.
[10] J. Sun, W. Abdulla, Palm vein recognition by combining curvelet transform and gabor filter, in: Biometric Recognition, Springer, 2013, pp. 314–321.
[11] Z. Zhang, S. Ma, X. Han, Multiscale feature extraction of finger-vein patterns based on curvelets and local interconnection structure neural network, in: International Conference on Pattern Recognition, IEEE, 2006, pp. 145–148.
[12] K.Y. Shin, Y.H. Park, D.T. Nguyen, K.R. Park, Finger-vein image enhancement using a fuzzy-based fusion method with gabor and retinex filtering, Sensors 14 (2) (2014) 3095–3129.
[13] N. Miura, A. Nagasaka, T. Miyatake, Feature extraction of finger-vein patterns based on repeated line tracking and its application to personal identification, Machine Vis. Appl. 15 (4) (2004) 194–203.
[14] N. Miura, A. Nagasaka, T. Miyatake, Extraction of finger-vein patterns using maximum curvature points in image profiles, IEICE Trans. Inform. Syst. 90 (8) (2007) 1185–1194.
[15] J. Yang, Y. Shi, Finger–vein roi localization and vein ridge enhancement, Pattern Recogn. Lett. 33 (12) (2012) 1569–1579.
[16] J. Yang, Y. Shi, Towards finger-vein image restoration and enhancement for finger-vein recognition, Inform. Sci. 268 (2014) 33–52.
[17] J.-C. Lee, A novel biometric system based on palm vein image, Pattern Recogn. Lett. 33 (12) (2012) 1520–1528.
[18] J. Yang, Y. Shi, J. Yang, L. Jiang, A novel finger-vein recognition method with feature combination, in: International Conference on Image Processing, IEEE, 2009, pp. 2709–2712.
[19] C.-L. Lin, K.-C. Fan, Biometric verification using thermal images of palm-dorsa vein patterns, IEEE Trans. Circ. Syst. Video Technol. 14 (2) (2004) 199–213.
[20] M.A. Olsen, D. Hartung, C. Busch, R. Larsen, Convolution approach for feature detection in topological skeletons obtained from vascular patterns, in: IEEE Symposium Series on Computational Intelligence, vol. 20, 2011.
[21] K. Wang, Y. Zhang, Z. Yuan, D. Zhuang, Hand vein recognition based on multi supplemental features of multi-classifier fusion decision, in: International Conference on Mechatronics and Automation, IEEE, 2006, pp. 1790–1795.
[22] A. Kumar, K.V. Prathyusha, Personal authentication using hand vein triangulation and knuckle shape, IEEE Trans. Image Process. 18 (9) (2009) 2127–2136.
[23] J. Uriarte-Antonio, D. Hartung, J. Pascual, R. Sanchez-Reillo, Vascular biometrics based on a minutiae extraction approach, in: International Carnahan Conference on Security Technology, IEEE, 2011, pp. 1–7.
[24] L. Wang, G. Leedham, D. Siu-Yeung Cho, Minutiae feature analysis for infrared hand vein pattern biometrics, Pattern Recogn. 41 (3) (2008) 920–929.
[25] D. Hartung, M.A. Olsen, H. Xu, C. Busch, Spectral minutiae for vein pattern recognition, in: International Joint Conference on Biometrics, IEEE, 2011, pp. 1–7.
[26] D. Hartung, M. Aastrup Olsen, H. Xu, H. Thanh Nguyen, C. Busch, Comprehensive analysis of spectral minutiae for vein pattern recognition, IET Biometr. 1 (1) (2012) 25–36.
[27] A.M. Badawi, Hand vein biometric verification prototype: a testing performance and patterns similarity, in: International Conference on Image Processing, Computer Vision, and Pattern Recognition, 2006, pp. 3–9.
[28] Y. Wang, K. Li, J. Cui, L.-K. Shark, M. Varley, Study of hand-dorsa vein recognition, in: Advanced Intelligent Computing Theories and Applications, Springer, 2010, pp. 490–498.
[29] J. Cross, C. Smith, Thermographic imaging of the subcutaneous vascular network of the back of the hand for biometric identification, in: 29th Annual International Carnahan Conference on Security Technology, IEEE, 1995, pp. 20–35.
[30] L. Wang, G. Leedham, A thermal hand vein pattern verification system, in: Pattern Recognition and Image Analysis, Springer, 2005, pp. 58–65.
[31] Z. Meng, X. Gu, Palm-dorsal vein recognition method based on histogram of local gabor phase xor pattern with second identification, J. Signal Process. Syst. (2013) 1–7.
[32] Y. Wang, T. Liu, J. Jiang, A multi-resolution wavelet algorithm for hand vein pattern recognition, Chinese Opt. Lett. 6 (9) (2008) 657–660.
[33] N. Otsu, A threshold selection method from gray-level histograms, Automatica 11 (1975) 285–296.
[34] K. Zuiderveld, Graphics Gems iv, Academic Press Professional, Inc., San Diego, CA, USA, 1994. Chapter: Contrast limited adaptive histogram equalization, pp. 474–485..
[35] P. Gupta, P. Gupta, Slap fingerprint segmentation using symmetric filters based quality, in: International Conference on Advances in Pattern Recognition, 2015.
[36] P. Gupta, P. Gupta, A dynamic slap fingerprint based verification system, in: International Conference on Intelligent Computing, 2014, pp. 812–818.
[37] P. Gupta, P. Gupta, Slap fingerprint segmentation, in: Fifth International Conference on Biometrics: Theory, Applications and Systems, IEEE, 2012, pp. 189–194.
[38] P. Gupta, P. Gupta, Fingerprint orientation modeling using symmetric filters, in: Proc. IEEE Winter Conference on Applications of Computer Vision, 2015.
[39] R. Jain, R. Kasturi, B. Schunck, Machine Vision, vol. 5, McGraw-Hill, New York, 1995.
[40] P. Gupta, P. Gupta, A vein biometric based authentication system, in: Information Systems Security, Springer, 2014, pp. 425–436.
[41] S. Chaudhuri, S. Chatterjee, N. Katz, M. Nelson, M. Goldbaum, Detection of blood vessels in retinal images using two-dimensional matched filters, IEEE Trans. Med. Imaging 8 (3) (1989) 263–269.

[42] S. Mallat, S. Zhong, Characterization of signals from multiscale edges, IEEE Trans. Pattern Anal. Machine Intell. 14 (7) (1992) 710–732.
[43] P. Gupta, P. Gupta, Extraction of true palm-dorsa veins for human authentication, in: Indian Conference on Computer Vision, Graphics & Image Processing, IEEE, 2014.
[44] Y.-B. Zhang, Q. Li, J. You, P. Bhattacharya, Palm vein extraction and matching for personal authentication, in: Advances in Visual Information Systems, Springer, 2007, pp. 154–164.
[45] P. Gupta, P. Gupta, An accurate finger vein based verification system, Digit. Signal Process. (2015).
[46] G. Xiong, Local normalization, 2005. <http://www.mathworks.in/matlabcentral/fileexchange/8303-local-normalization>.
[47] P. Gupta, P. Gupta, A robust singular point detection algorithm, Appl. Soft Comput. (2015).
[49] D. Rueckert, L.I. Sonoda, C. Hayes, D.L. Hill, M.O. Leach, D.J. Hawkes, Nonrigid registration using free-form deformations: application to breast mr images, IEEE Trans. Med. Imaging 18 (8) (1999) 712–721.
[50] L. Lam, S.-W. Lee, C.Y. Suen, Thinning methodologies-a comprehensive survey, IEEE Trans. Pattern Anal. Machine Intell. 14 (9) (1992) 869–885.
[51] M. Soni, P. Gupta, A robust vein pattern-based recognition system, J. Comput. 7 (11) (2012) 2711–2718.
[52] B.V. Kumar, A. Mahalanobis, R.D. Juday, Correlation Pattern Recognition, vol. 27, Cambridge University Press, Cambridge, 2005.
[53] R.M. Bolle, N.K. Ratha, S. Pankanti, Error analysis of pattern recognition systems the subsets bootstrap, Comput. Vis. Image Understand. 93 (1) (2004) 1–33.
[54] A. Buades, B. Coll, J.-M. Morel, A review of image denoising algorithms, with a new one, Multiscale Model. Simul. 4 (2) (2005) 490–530.
[55] R.C. Gonzalez, R.E. Woods, Digital Image Processing, 3rd ed., Prentice-Hall, Inc., Upper Saddle River, NJ, USA, 2006.
[56] J.L. Horner, P.D. Gianino, Phase-only matched filtering, Appl. Opt. 23 (6) (1984) 812–816.
[57] M. Ferrer, A. Morales, L. Ortega, Infrared hand dorsum images for identification, Electron. Lett. 45 (6) (2009) 306–308.
[58] X. Li, X. Liu, Z. Liu, A dorsal hand vein pattern recognition algorithm, Third International Congress on Image and Signal Processing, vol. 4, IEEE, 2010, pp. 1723–1726.
[59] Y. Wang, W. Liao, Hand vein recognition based on feature coding, in: Seventh Chinese Conference on Biometric Recognition, Springer, 2012, pp. 165–175.
[60] D. Maltoni, D. Maio, A.K. Jain, S. Prabhakar, Handbook of Fingerprint Recognition, Springer, 2009.
[61] GDPSvein database (GPDS100VeinsCCDcylindrical database), <http://www.gpds.ulpgc.es/download/>.
[62] G. Park, S. Kim, Hand biometric recognition based on fused hand geometry and vascular patterns, Sensors 13 (3) (2013) 2895–2910.